remote sensing

MDPI

Article

On the Applicability of Galileo FOC Satellites with Incorrect Highly Eccentric Orbits: An Evaluation of Instantaneous Medium-Range Positioning

Jacek Paziewski, Rafal Sieradzki and Pawel Wielgosz *

Institute of Geodesy, University of Warmia and Mazury in Olsztyn, 10-719 Olsztyn, Poland; jacek.paziewski@uwm.edu.pl (J.P.); rafal.sieradzki@uwm.edu.pl (R.S.)

* Correspondence: pawel.wielgosz@uwm.edu.pl

Received: 20 December 2017; Accepted: 26 January 2018; Published: 30 January 2018

Abstract: This study addresses the potential contribution of the first pair of Galileo FOC satellites sent into incorrect highly eccentric orbits for geodetic and surveying applications. We began with an analysis of the carrier to noise density ratio and the stochastic properties of GNSS measurements. The investigations revealed that the signal power of E14 & E18 satellites is higher than for regular Galileo satellites, what is related to their lower altitude over the experiment area. With regard to the noise of the observables, there are no significant differences between all Galileo satellites. Furthermore, the study confirmed that the precision of Galileo data is higher than that of GPS, especially in the case of code measurements. Next analysis considered selected domains of precise instantaneous medium-range positioning: ambiguity resolution and coordinate accuracy as well as observable residuals. On the basis of test solutions, with and without E14 & E18 data, we found that these satellites did not noticeably influence the ambiguity resolution process. The discrepancy in ambiguity success rate between test solutions did not exceed 2%. The differences between standard deviations of the fixed coordinates did not exceed 1 mm for horizontal components. The standard deviation of the L1/E1 phase residuals, corresponding to regular GPS and Galileo, and E14 & E18 satellite signals, was at a comparable level, in the range of 6.5–8.7 mm. The study revealed that the Galileo satellites with incorrect orbits were fully usable in most geodetic, surveying and many other post-processed applications and may be beneficial especially for positioning during obstructed visibility of satellites. This claim holds true when providing precise ephemeris of satellites.

Keywords: Galileo; GNSS; RTK; satellite positioning

1. Introduction

Galileo—the first European global navigation satellite system providing worldwide positioning, navigation and timing services—has been under extensive development since the early 2000s. The first two experimental satellites—GIOVE-A and GIOVE-B—were launched in 2005 and 2008, respectively. The satellites were the part of the Galileo System Test Bed (GSTB) [1]. After the initial delay of the programme, in recent years we can observe acceleration of the system development. The final constellation will comprise 30 satellites in total, evenly spread on three medium earth orbits including 24 operational plus two spare satellites per plane defining 24/3/1 Walker constellation [2,3]. At present (October 2017) the Galileo constellation consists of 18 satellites; however, this includes one with "not unusable", two with "testing" and one with "not available" status. The current constellation consists of satellites belonging to in-orbit validation (IOV) and full operational capability (FOC) phases. The former phase, which has already been accomplished, used four satellites launched in 2011 and 2012 to validate the system. The latter comprises operational satellites launched from 2014 onwards.

On 22 August 2014, the first two FOC satellites (GSAT0201-E18 and GSAT0202-E14), also named Doresa and Milena, respectively, were unintentionally injected into a wrong orbit. The failure was caused by a technical problem—specifically, by an interruption of propellant supply to the thrusters. On the next day, it was announced that the actual inclination of these satellites' orbits is ~5° lower than the nominal one. Furthermore, the eccentricity of the orbit reached 0.29, which is much higher than the nominal one of 0.0002. Therefore, these satellites were in December 2014 and March 2015 moved by a series of correction manoeuvres into an improved, but still highly eccentric, orbit. This, however, consumed a significant amount of the on-board fuel. Afterwards, the satellites started transmission of the navigational signals [4]. Selected parameters of the actual and nominal E14 & E18 Galileo orbits are listed in Table 1.

The open question is the potential contribution of the first pair of FOC satellites to the Galileo services and applications. Due to format restrictions of the orbital parameters, E14 and E18 satellites are not included in the broadcast navigation message. Specifically, actual deviations of the semimajor axis and eccentricity exceed the nominal values by far over the limit. Accepting the premise that the maximum value of the eccentricity applied to the broadcast navigation message is 0.03125, the actual value exceeds the limit and reaches the level of 0.16. The nominal value of the semimajor axis (29,600 km) deviates by a value of 1620 km, which also exceeds the limit of 87 km. These facts seem to prevent the application of the E14 & E18 satellites to real-time solutions. Notwithstanding this, the satellites' observations may be applied to post-processing applications, since several GNSS analysis centres provide post-mission products such as satellite clock corrections and orbits. As former studies showed, the quality of such E14 & E18 orbits may be considered as not worse than that of nominal FOC and IOV satellites [5]. Moreover, the eccentricity of the satellite orbits offers several possibilities for scientific applications including general relativity studies. It is recognised that an elliptic orbit of a satellite causes a periodic modulation of the gravitational redshift [6]. This phenomenon may be investigated by taking advantage of the high stability of the on-board H-maser clocks and the high eccentricity of the E14 & E18 orbits [7]. Furthermore, satellite observations may be used in a number of post-mission surveying, geodetic, and geodynamics applications, which is, in a sense, the goal of this paper.

Table 1. Selected parameters of E14 and E18 Galileo FOC satellites' orbits [8].

PRN Number/NORAD ID **Launch Date** **Signal Transmission Date**	**Nominal Orbit**	**GSAT0201 (5-Doresa)** **E18/40128** **22 August 2014** **29 November 2014**	**GSAT0202 (6-Milena)** **E14/40129** **22 August 2014** **17 March 2015**
Semi-major axis (km)	29,599.8	27,978	27,978
Eccentricity	0.0001	0.15601	0.15167
Revolution period (h)	14.08	12.97	12.97
Inclination (°)	56	49.775	49.874
Minimum orbital height (km)	23,220	17,382	17,382
Maximum orbital height (km)	23,240	25,818	25,818

Since the initial phases of the Galileo program, the observational data were applied and analysed in several ways. This includes the signal analysis and positioning performance. The former studies of Galileo signals were devoted to phase and code noise, multipath, and cross-correlation [9–13]. The latter issue, applied to both single-system and multi-constellation single-point positioning, was investigated in [14–18]. Moreover, at this point we should acknowledge several studies devoted to precise positioning including both absolute (PPP) and relative (RTK) algorithm development and performance assessment. Example of single-system and combined PPP results may be found in [19–23], while the application of GIOVE and IOV Galileo signals to RTK was examined in [13,24]. In [25], single-frequency RTK positioning was analysed; in [26] selected methods for GPS + Galileo signals integration were studied and assessed, while [27] was devoted to Galileo IOV + FOC. At this point, it should be noted that the aforementioned studies did not include Galileo E14 and E18 satellites.

Moreover, most of these studies, based on real signals, were also limited to close-range RTK—single short baselines. Therefore, in order to extend knowledge in this field, in this paper we analyse the potential use of Galileo satellites with highly eccentric orbits in medium-range instantaneous RTK positioning.

Nowadays, RTK positioning is considered a highly effective and reliable method of precise coordinate determination and so is a standard in many commercial and scientific applications. However, the starting point, which was a single-baseline single-system RTK positioning, suffered from several disadvantages such as limited baseline length and longer time to fix during higher ionosphere activity. Within the last decades, several advances in the RTK algorithms were introduced. These led to the development of the network-RTK mode, utilising atmospheric corrections derived from active reference networks. Taking advantage of these new algorithms, it was possible to extend the distance between reference sites and user receivers, and thus extend the service coverage area. This resulted in so-called wide area RTK, with baseline length up to dozens and even hundreds of kilometres (see [28–31]).

Simultaneously, to support Positioning, Navigation and Timing applications (PNT), unprecedented interest was directed to algorithm and methodology development for combining multi-constellation signals. Several contributions were devoted not only to algorithm development and assessment [26,32], but also to characterisation of the inter GPS-Galileo system biases both in precise relative (RTK) and absolute methods (PPP) [33–37]. Thus, the RTK method can be considered as under extensive development and being used for a growing number of applications.

The main objective of this paper is to evaluate the applicability of the E14 & E18 satellites to precise GNSS positioning. In this contribution we focus on relative kinematic positioning as an instantaneous solution in multi-baseline mode. The prerequisite of precise relative positioning is the correct ambiguity resolution. As expected, reliable single-epoch ambiguity resolution is obviously challenging [38–41]. On the other hand, such an approach is resistant to cycle-slips, and may be beneficial for better assessing the established and compared positioning scenarios.

To present a comprehensive study, in the following section we start with the analysis of code and phase signals noise, with special attention paid to E14 & E18 satellites. Such analysis may be beneficial for establishing, e.g., an advanced stochastic model of positioning [42]. The characteristic of stochastic properties is followed by presentation of the observation model of multi-constellation relative kinematic positioning. Furthermore, the performance of the instantaneous multi-station medium-range positioning is assessed using single-system or combined GPS + Galileo dual-frequency data. The computations were performed using GNSS data processing software developed at the University of Warmia and Mazury in Olsztyn. In the last section, a summary and conclusions are provided.

2. Analysis of Signal Power and Noise

It can be expected that varying the height of E14 and E18 satellites should influence satellite signal strength and may lead to some modifications of its stochastic properties. Thus, in this work the positioning performance was preceded by evaluation of phase and code observational noise for GPS and Galileo measurements, with special attention to E14 and E18 satellites. In order to ensure full coverage of elevation angle domain by observations, raw data with 1 s interval were processed during a period of two weeks (3–16 October 2017). The noise analysis involved stations used subsequently for evaluation of precise positioning, i.e., BYCE, CHLE, IAWA and OLSZ. The experiment was based on data collected at four sites in Poland (Figure 1). All these sites are equipped with Trimble NETR9 receivers. Three of them are equipped with geodetic TRM115000.00 antennas, whereas the last one (OLSZ) uses a choke-ring TRM59900.00 antenna.

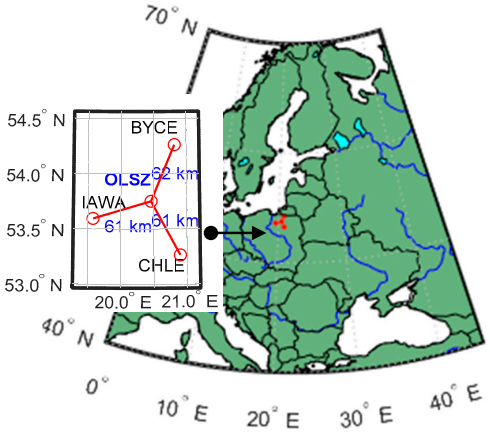

Figure 1. Baselines and stations processed in the experiment.

2.1. Signal Power

It is well known that the observational noise is basically related to the power of the satellite signal at the receiver, and the stochastic properties of GNSS data can be described as a function of this indicator [43,44]. Furthermore, it was also confirmed that the carrier to noise density ratio (C/N0) for BDS-IGSO and GEO satellites, which are characterised by a much higher altitude, is 3–4 dB-Hz lower than common BDS-MEO satellites [45,46]. Thus, the starting point of the investigations given in this section is the analysis of the carrier to noise density ratio for E14 and E18 satellites registered at different altitudes. For this purpose, we computed 5-min mean values of C/N0 at two frequencies, E1 and E5a, for all FOC Galileo satellites. Subsequently, the reference level of C/N0 for common ones was determined through averaging in 10° bins of elevation angle. The summary of these computations for two selected stations, IAWA and OLSZ (two top and two bottom panels, respectively), is given in Figure 2. According to the results, it can be confirmed that registered C/N0 values depend on the varying radius of highly eccentric orbits. At high elevations, where satellites were practically at minimal altitudes (~17,000–18,000 km), C/N0 increased from 1 and 5 dB-Hz. Interestingly, at the first frequency (Figure 2, left column), strong discrepancies between results for satellites E14 and E18 are observed, whereas at E5a (right column) they are consistent to each other and equal about 2.5 dB-Hz. This divergence was detected at all stations and seems to be related to the different power of E1 signal emitted by both satellites. At low elevations the enhancement of C/N0 did not exceed 2 dB-Hz in all cases. Furthermore, the signal strength values registered at maximal height, which was similar to the nominal one of Galileo orbit, are coincident with average C/N0 pattern obtained for remaining satellites. The common difference between levels of C/N0 for both stations (~3 dB-Hz) seems to be connected with different antenna type. The results for sites BYCE and CHLE, equipped the same as IAWA, not included here, are generally consistent with the latter.

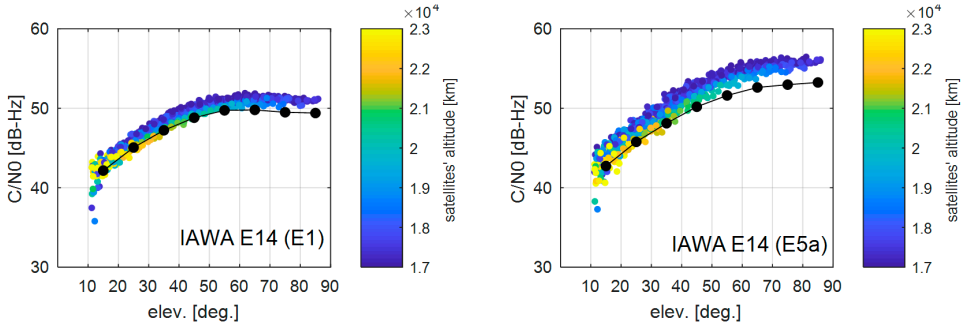

Figure 2. *Cont.*

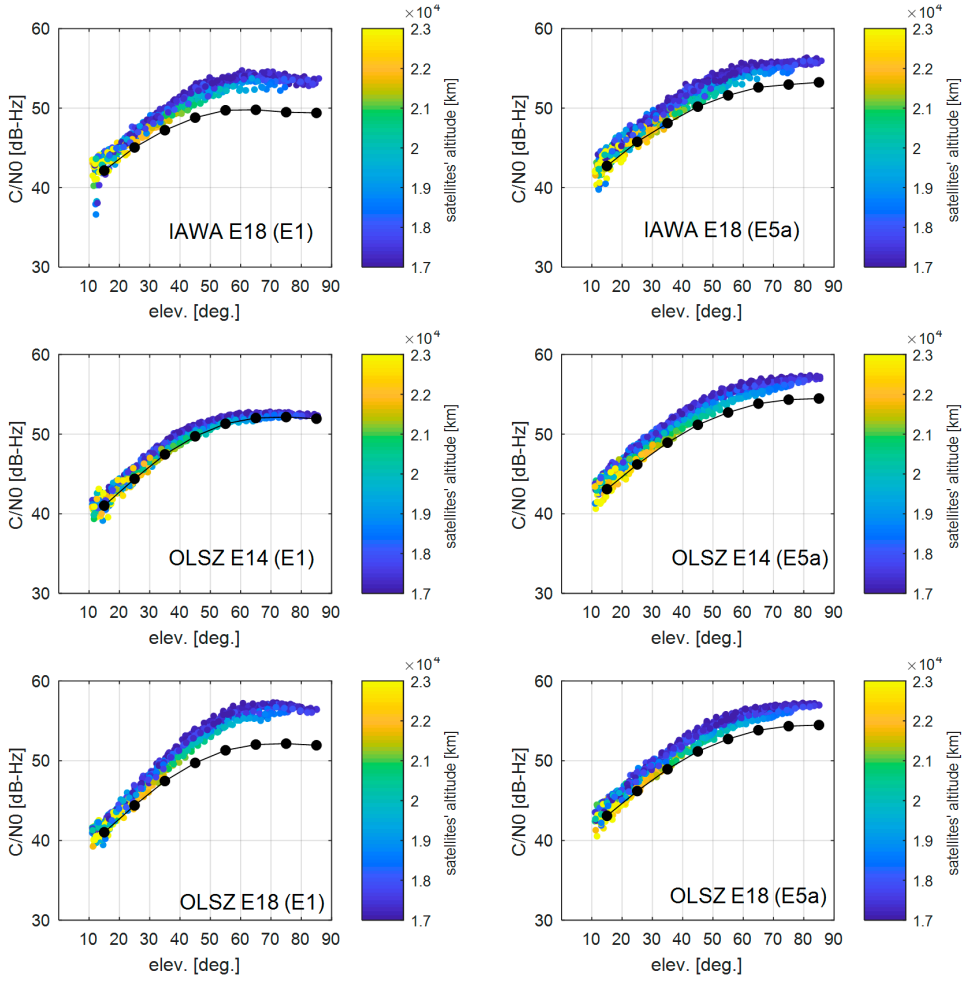

Figure 2. Carrier-to-noise density ratio of the Galileo E14 and E18 signals on different frequencies as function of satellite elevation and altitude (two top panels—IAWA, two bottom panels—OLSZ). Black lines correspond to average C/N0 for Galileo satellites signals (E1 or E5a) at particular station.

2.2. Code Measurement Noise

The precision of code observations is generally limited by the combined influence of receiver noise and site-specific multipath effect. The aggregate impact of both these factors is usually evaluated using multipath combinations, which are formed from dual-frequency code and phase observations [47]. Under the assumption $f_1 > f_2$, the multipath combinations for satellite i and receiver k can be written as follows:

$$MP1 = P^i_{k,f_1} - \left(1 + \frac{2}{\mu - 1}\right)\lambda_{f_1}\varphi^i_{k,f_1} + \left(\frac{2}{\mu - 1}\right)\lambda_{f_2}\varphi^i_{k,f_2} \approx M^i_{k,P,f_1} + \epsilon^i_{k,P,f_1} + B^i_{k,MP1} \quad (1)$$

$$MP2 = P^i_{k,f_2} - \left(\frac{2\mu}{\mu - 1}\right)\lambda_{f_1}\varphi^i_{k,f_1} + \left(\frac{2\mu}{\mu - 1} - 1\right)\lambda_{f_2}\varphi^i_{k,f_2} \approx M^i_{k,P,f_2} + \epsilon^i_{k,P,f_2} + B^i_{k,MP2} \quad (2)$$

where P and φ are dual-frequency code and phase observables, respectively; λ is the signal wavelength; M and ϵ denote multipath and noise effects affected code measurements; B is a constant factor including ambiguity terms and hardware delay biases (eliminated by the subtracting the mean values of $MP1$ or $MP2$ time series for entire arc; and μ is the constant factor applied for conversion of the ionosphere delay on first frequency into that on second frequency according to the formula:

$$\mu = f_1^2 / f_2^2. \quad (3)$$

The above equations were applied to generate time series of dual-frequency multipath combinations for all observational arcs. For this purpose we used code observations C1C, C2W (GPS), C1X, C5X (Galileo) and the corresponding phase data. Subsequently, their RMSs in 10° bins of elevations were computed separately for GPS, common Galileo, and satellites with eccentric orbits. The results obtained for two selected stations are presented in Figure 3.

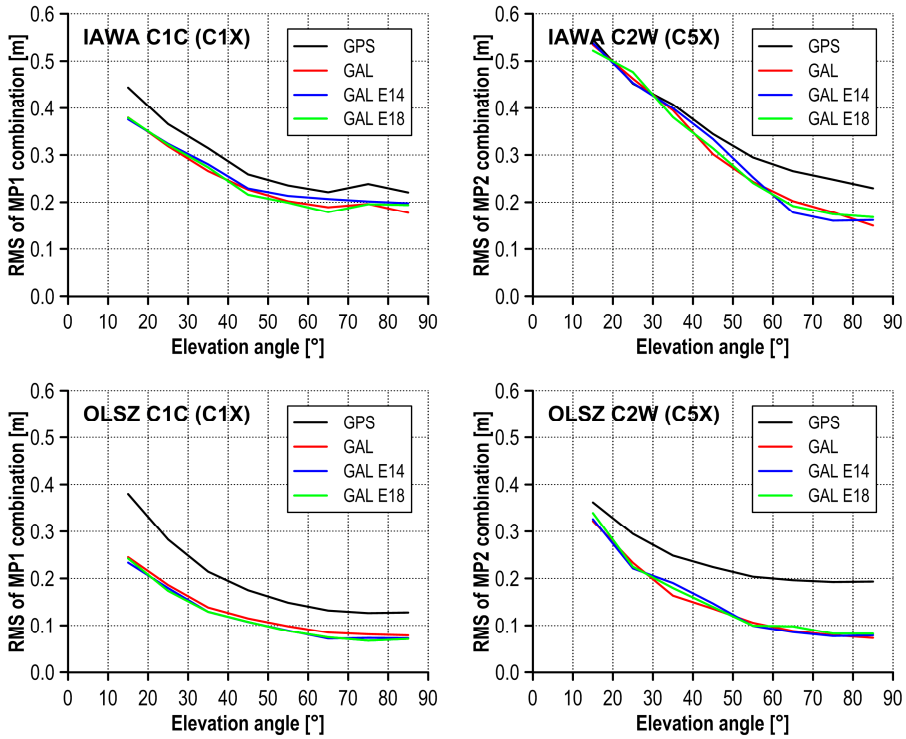

Figure 3. Variation of code noise and multipath with elevation at stations IAWA (top panel) and OLSZ (bottom panel).

With regard to results obtained for E14 and E18 satellites, one can conclude that the precision of their code observations is at the same level as for other Galileo satellites. Comparing only European satellites, the highest differences in elevation patterns did not exceed 3 cm and seem to be related to site-specific multipath effect. On the other hand, the results demonstrated significant distinctions between stations and systems. The former issue is a consequence of choke ring antenna installed at OLSZ station, which allows improved multipath mitigation. Thus, errors of code observables are significantly lower than at the IAWA site. The improvement at high elevations reaches about 10 cm for both Galileo (C1X) and GPS (C1C) code signals. Only in the case of C2W observations is the decrease of code observation errors for OLSZ site much lower, not exceeding 5 cm. Furthermore, the results basically confirm that the precision of Galileo code observations outperforms those of the GPS ones. RMS values of MP1 and MP2 combinations at high elevations for the European system are at the level of 0.19 m, 0.16 m (IAWA) and 0.08 m, 0.08 m (OLSZ). The corresponding values for GPS are 0.22 m, 0.23 m and 0.13 m, 0.19 m, respectively. The analysis executed for the remaining sites (BYCE and CHLE) showed a similar precision of code observations as for IAWA station (see Table 2). Analysing these results, one can also conclude that the precision of E5a code measurements at sites with common antennas (BYCE, CHLE, IAWA) is higher than for the E1 signal. This improvement, observed for all three cases, varies between 0.02 m and 0.06 m.

Table 2. RMS of dual-frequency multipath combinations at zenith (m).

Station	GPS		Galileo (Except #14 and E18)		Galileo E14		Galileo E18	
	*MP*1	*MP*2	*MP*1	*MP*2	*MP*1	*MP*2	*MP*1	*MP*2
BYCE	0.20	0.21	0.16	0.14	0.16	0.13	0.16	0.13
CHLE	0.21	0.22	0.19	0.13	0.17	0.13	0.18	0.13
IAWA	0.22	0.23	0.18	0.15	0.20	0.16	0.19	0.17
OLSZ	0.13	0.19	0.08	0.07	0.07	0.08	0.07	0.08

2.3. Phase Measurement Noise

The analysis of phase noise at a particular frequency is usually performed with zero or ultra-short baselines, which allows for elimination of short-term variations of atmospheric influence. However, the stations used in the given experiment belong to active reference networks and are distant from each other by a few tens of kilometres. In such a case the combined weighted phase noise can be derived from single-station data using triple-frequency combinations. In our case it was realised using the difference of two ionosphere-free combinations (DIF) according to the following equation [12,45]:

$$\begin{aligned} DIF\left(\varphi^i_{k,f_1}, \varphi^i_{k,f_2}, \varphi^i_{k,f_3}\right) &= IF\left(\varphi^i_{k,f_1}, \varphi^i_{k,f_2}\right) - IF\left(\varphi^i_{k,f_1}, \varphi^i_{k,f_3}\right) \\ &= \left(\frac{f_1^2}{f_1^2-f_2^2} - \frac{f_1^2}{f_1^2-f_3^2}\right)\lambda_{f_1}\varphi^i_{k,f_1} - \frac{f_2^2}{f_1^2-f_2^2}\lambda_{f_2}\varphi^i_{k,f_2} + \frac{f_3^2}{f_1^2-f_3^2}\lambda_{f_3}\varphi^i_{k,f_3} \end{aligned} \quad (4)$$

This triple-frequency combination theoretically eliminates all geometric factors and influence of the first-order term of ionospheric refraction. Thus, the right side of the equation should contain aggregated weighted phase noise, constant factor including ambiguity term, hardware delay and inter-frequency biases The last parameter was recognised and investigated in GLONASS (due to satellite individual frequencies) and GPS signals. However, it was reported in [12,48] that for the latter system such data are affected by variations of inter-frequency bias, which have to be eliminated.

In this work triple-frequency combinations were created taking advantage of L1, L2, L5 and E1, E5a, E5b signals of GPS and Galileo systems, respectively. The long-term variations associated with inter-frequency bias, also observed in our case, were removed using a fourth-order polynomial. The further algorithm of DIF combination data processing was analogous as in the case of multipath combinations. A summary of phase noise variations with elevation angle is presented in Figure 4.

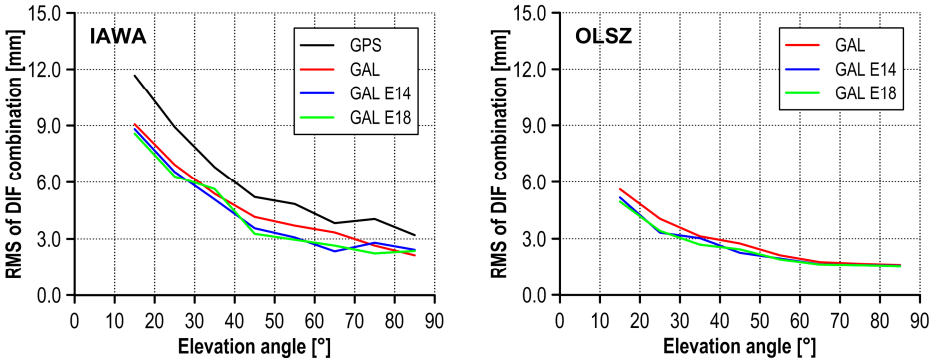

Figure 4. Variation of phase noise and multipath (DIF) with elevation at stations IAWA (left panel) and OLSZ (right panel).

Looking at these results, it can be observed that DIF phase noise for E14 and E18 is slightly lower (up to 1 mm) than for the other Galileo satellites. On the other hand, this improvement is detectable only at selected elevations (mainly low) and is probably an effect of the lower multipath in these cases.

At high elevations the differences do not exceed 0.3 mm and 0.1 mm at IAWA and OLSZ, respectively. The results from stations with better equipment prove that the level of phase noise for both analysed satellites is the same as for the others. The comparison of RMS values for IAWA and OLSZ sites confirms that applying a choke ring antenna reduces the phase multipath in the entire elevation angle domain. As a consequence, RMS of DIF combination declines from 2.3 mm and 8.8 mm to 1.6 mm and 5.0 mm at high and low elevations, respectively. Unfortunately, OLSZ station did not record the third GPS frequency, and thus the discussed results are given for IAWA station only. Taking into account ionosphere-free combination coefficients, it can be expected that RMS of DIF for the GPS system should be higher, but only by about 5% (assuming the same precision at all frequencies). However, in the case of IAWA this deterioration is about 25%, suggesting that Galileo phase observations are less noisy. These findings need further investigation.

3. Instantaneous Multi-Constellation Relative Positioning: Methodology and Performance

Our first goal in this section is to briefly present a multi-constellation geometry-based relative positioning model. This is followed by an empirical evaluation of the instantaneous positioning with a focus on the application of Galileo E14 and E18 satellites.

3.1. Loosely Combined Relative Positioning Model with Parameterised Ionospheric Delays

Nowadays, there are several functional models for combined processing of multi-constellation signals in a relative mode with double-differences (DD) (see [26]). Basically, we can distinguish between two general approaches: intra-system and inter-system combination. The former uses separate pivot satellite for each constellation when forming double-differenced observables. Thus, the observational model is free from the DD observables formed across constellations. This methodology can be considered a classical approach, applied commonly to constellations with no overlapping frequencies.

The latter approach, termed tightly integrated or tightly coupled, uses a single common pivot satellite for all constellations. As a result, in this positioning model there are both intra-system and inter-system DD observables (mixed). Such an approach can be especially beneficial in urban canyons with limited satellite visibility, due to a higher number of DD observables in comparison to the intra-system combination. When using the tight integration we do not lose one satellite as pivot per constellation. The prerequisite of application of the tight integration is the presence of common frequencies in combined constellation, such as L1/E1 and L5/E5a in GPS and Galileo [49].

This model can strengthen the solution; however, it requires handling of inter-system biases. Specifically, in the relative mode these biases are differential values (differential ISBs). As studies show, the phase and code differential ISBs may be considered stable [37]. This creates an opportunity for priori calibration of the biases and further correction of observations. As a result, inter-system phase ambiguities for overlapping frequencies may be fixed to their integer values. At this point we should also highlight the most recent contributions considering an inter-system model with no overlapping frequencies. A tightly combined GPS + BDS RTK model with real-time estimation of differential ISB was proposed in [50]. Nevertheless, as studies show, both tight and loose coupling may provide comparative performance, especially in the case of a high number of tracked satellites [26,50]. Thus, considering the above, in this study we apply an intra-system model for assessing the performance of the relative kinematic positioning with the use of Galileo E14 & E18 satellites.

Over the last decades several approaches were recognised for modelling of the ionospheric delay in relative GNSS positioning. Their application mainly depends on the baseline length, state of the ionosphere, positioning mode or session length. Among others, one highly effective approach is the ionosphere weighted model, commonly applied for medium- and long-range RTK [38,39,51–54] as well as instantaneous positioning [40,55]. The ionosphere weighted model can be considered a generalised approach to ionosphere delay parameterisation, taking into account information on both a priori values of ionosphere delays and its stochastic properties. Thus, the estimated DD ionospheric delays are weighted in the model estimation process by the application of the pseudo-observables, which allows

for constraining parameters using a priori variance factors. Thanks to the above, it is possible to tune these parameters to the expected values of the factual double differenced ionospheric delays. If we, however, do not introduce a priori information of the ionosphere delays, the model can be labelled the ionosphere float. On the other hand, positioning supported with ionospheric corrections considered as errorless is commonly termed the ionosphere fixed model [56]. The latter approach is, however, not applied in this study, since we take advantage of ionosphere float model.

The relative positioning model based on geometry with parameterised ionospheric delays is given in Equation (5). The equations are presented for dual frequency phase and code observables; however, the model may be extended for multi-frequency signals accordingly [32]:

$$\begin{cases} \lambda_{f_1}\varphi^{ij}_{kl,f_1} = \rho^{ij}_{kl} + T^{ij}_{kl} - I^{ij}_{kl} + \lambda_{f_1}N^{ij}_{kl,f_1} + \epsilon^{ij}_{kl,\varphi,f_1} \\ P^{ij}_{kl,f_1} = \rho^{ij}_{kl} + T^{ij}_{kl} + I^{ij}_{kl} + \epsilon^{ij}_{kl,P,f_1} \\ \lambda_{f_2}\varphi^{ij}_{kl,f_2} = \rho^{ij}_{kl} + T^{ij}_{kl} - \mu I^{ij}_{kl} + \lambda_{f_2}N^{ij}_{kl,f_2} + \epsilon^{ij}_{kl,\varphi,f_2} \\ P^{ij}_{kl,f_2} = \rho^{ij}_{kl} + T^{ij}_{kl} + \mu I^{ij}_{kl} + \epsilon^{ij}_{kl,P,f_2} \end{cases} \tag{5}$$

where λ is the signal wavelength, φ is the carrier phase observable in cycles, P is the code pseudorange, ρ denotes the geometric satellite to receiver range, N is the integer ambiguity, superscripts i, j and k, l states for satellites and stations, respectively, subscripts f_1 and f_2 correspond to the first and second applied frequencies, I is the ionospheric delay at the first frequency, ϵ denotes multipath and observation noise.

T is the tropospheric delay, the double differenced value of which can be denoted as:

$$T^{ij}_{kl} = \left(\alpha^i_k ZTD_k - \alpha^j_k ZTD_k - \alpha^i_l ZTD_l + \alpha^j_l ZTD_l\right), \tag{6}$$

where ZTD is the tropospheric total zenith delay and α is the troposphere mapping function coefficient. ZTDs may be introduced as known values derived from global tropospheric models (troposphere fixed model) or treated as constrained parameters whose a priori values are corrected via estimation of the corrections (troposphere-weighted model).

Since the linearized equations are formed independently for each constellation, there are no inter-system DD observables. The vector of unknowns is expressed as follows:

$$x = \left[\delta X_k, \delta Y_k, \delta Z_k, \delta X_l, \delta Y_l, \delta Z_l, \delta ZTD_k, \delta ZTD_l, N^{ij}_{kl} \ldots N^{ij}_{kl}, I^{ij}_{kl} \ldots I^{ij}_{kl}\right]^T, \tag{7}$$

where $\{\delta X_k, \delta Y_k, \delta Z_k, \delta X_l, \delta Y_l, \delta Z_l\}$ are the corrections to a priori geocentric coordinates of the stations, $\{\delta ZTD_k, \delta ZTD_l\}$ are the residual zenith tropospheric delays, $\left\{N^{ij}_{kl} \ldots N^{ij}_{kl}\right\}$ denotes the set of phase ambiguities for selected DD intra observables and, finally, $\left\{I^{ij}_{kl} \ldots I^{ij}_{kl}\right\}$ denotes the set of epoch-specific DD ionospheric delays.

The final solution with resolved double-differenced ambiguities is performed via a four-step procedure: (1) the float solution; (2) the ambiguity resolution; (3) the ambiguity validation; (4) the fixed solution obtained via parameter update, taking into account fixed ambiguities from step (2). The details of the processing strategy are listed in Table 3.

Table 3. Processing strategy and session summary.

Date and Time of Session	**3–5 October 2017 00:00–24:00 UTC**
Baselines' lengths	61–62 km
GNSS constellations	GPS & Galileo
Observation types	dual frequency phase and pseudorange
Frequencies	L1 & L2 (GPS), E1 & E5a (Galileo)
Session length & solution	Instantaneous (single-epoch) relative solution
# of solutions per day	288 independent single-epoch solution per day (@300 s)
Tropospheric delay mitigation	a priori values from Modified Hopfield + GMF mapping function + tightly constrained estimation of the residual ZTD
Ionospheric delay mitigation	constrained estimation of DD first-order ionospheric delays (ionosphere float model)
Elevation cut-off angle	10°
Ephemeris	Precise final from CODE (COM) [57]
Observation weighting scheme	Elevation-dependent
Ambiguities handling	Fixed to integers with M-Lambda [58] and validated with W-ratio [59]
A priori standard deviation of undifferenced observations	0.2 m and 0.002 m for code and phase (E1/L1), respectively $\sigma_{L2} = \sigma_{L1} \cdot \lambda_{L2}/\lambda_{L1}$ $\sigma_{E5a} = \sigma_{L1} \cdot \lambda_{E5a}/\lambda_{L1}$
Estimation method	least squares adjustment with a priori parameter constraining (single-epoch)

3.2. Performance Assessment of Precise Positioning with Focus on E14 and E18 Galileo Satellites

3.2.1. Data Selection & Experiment Design

As stated previously, the hypothesis of the applicability of E14 and E18 satellites to positioning was verified on the basis of a multi-baseline, single-epoch RTK solution. For this purpose, the mathematical model given in Section 3.1 was applied to dual-frequency observations (L1/L2 & E1/E5a). The distribution of stations and test baselines used in the experiment is presented in Figure 1. We used one station as a simulated rover receiver (OLSZ), as well as three surrounding permanent stations serving as reference sites (IAWA, CHLE, BYCE), being a part of the VRSNet active reference network [60]. As a consequence, the baselines were of similar length and reached ~60 km. The observational data covered three days, 3–5 October 2017, and were sampled at 30 s intervals.

All sites were occupied by Trimble NETR9 receivers. BYCE, IAWA and CHLE sites were equipped with TRM115000.00 antennas, while at OLSZ station a choke ring model TRM59900.00 was used. Due to the lack of antenna phase centre offset and variation models for the Galileo E5a, E5b, E5 and E6 signals, the correction values corresponding to GPS L2 signals were applied. We believe that this may have a small impact on the positioning results due to the use of Galileo E5a observables. Nevertheless, at this time there is no better solution to this problem. Several processing scenarios were established for the experimental verification of the hypothesis (see Table 4). The first and second scenarios apply a single system: GPS or Galileo. The third scenario takes advantage of a combined model including Galileo satellites on incorrect orbits (E14 & E18). The last strategy is based on a combined solution; however, it excludes these two satellites. By analysing the results of the last two scenarios, we evaluated the impact of Galileo E14 & E18 on the performance of the precise positioning.

Table 4. Processing scenarios.

#	**Constellations**
1.	GPS
2.	Galileo
3.	Combined GPS + Galileo with E14 and E18
4.	Combined GPS + Galileo without E14 and E18

The performance assessment was based on several indicators of solution quality related to the ambiguity resolution—coordinate domains as well as observable residuals. The empirical ambiguity resolution success rate (ASR) was used for the evaluation of the ambiguity resolution process. This indicator was computed as a ratio of epochs with correctly fixed ambiguities with respect to the number of processed epochs. The quality of the fixed solution in the coordinate domain was based on the standard deviation (*std*) of coordinate residuals with respect to the target (reference) position. In the residual domain we characterised descriptive measures such as standard deviation. This description is also presented in residual histograms.

3.2.2. Geometry and Configuration of the Satellites during the Experiment

Figure 5 depicts the number of tracked satellites and corresponding PDOP values at Olsztyn during three days of processed data. The values are given for GPS and Galileo, as well as for a combined solution. As can be seen from the figure, the number of visible GPS satellites varied from five to 11; however, most of the time their number was in the range of 8–10. As a consequence, the PDOP values in most cases did not exceed the level of 2.5. This indicates relatively good conditions in terms of the geometric distribution of satellites. In the case of a combined solution, the PDOP values were obviously lower, in most cases below 2. On the other hand, judging on the basis of the number of Galileo satellites, one can expect a significant deterioration of the solution based solely on this constellation. With the current Galileo constellation, the number of satellites most of the time did not exceed six, but some periods accidentally reached seven or eight (Figure 5 solid green line). However, there were time intervals when the number of satellites equalled five or less; this accounted for 37% and 28% of the time, respectively. Thus, PDOP reached a significantly higher level than in the case of the GPS constellation. For 25% of the time, PDOP for the Galileo system was higher than 5 (Figures 5 and 6). Therefore, we can conclude that the geometric distribution of the Galileo satellites above the area of interest was not favourable for positioning, especially regarding the single-epoch mode.

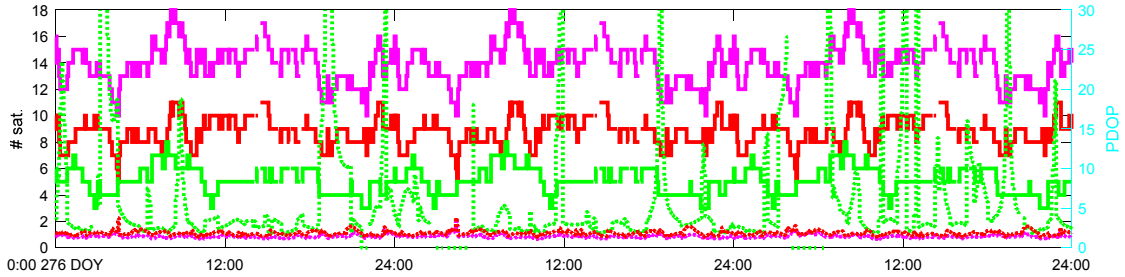

Figure 5. Number of tracked satellites (solid lines) and PDOP (dotted lines) corresponding to GPS-only constellation—red, Galileo-only constellation—green, GPS + Galileo—magenta).

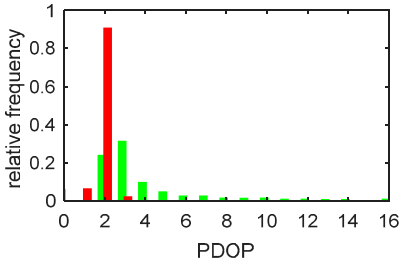

Figure 6. Histogram of PDOP values during experimental period. GPS constellation—red, Galileo constellation—green.

Figure 7 presents sky plots of the Galileo and GPS constellations over the area of interest. We can clearly see from the figure the deviation of E14 and E18 altitudes from the nominal values (dark blue

lines). While the nominal altitude of Galileo satellites reaches over ~23,200 km, E14 and E18 satellites were tracked at a significantly lower height above the Earth (below 18,000 km). Moreover, when the E14 and E18 satellites are close to their minimal orbital height, they are observed at high elevation angles at experiment localisation. As is well known, GPS orbits with altitude lower than Galileo equal ~20,200 km, hence in Figure 7 they are marked with azure.

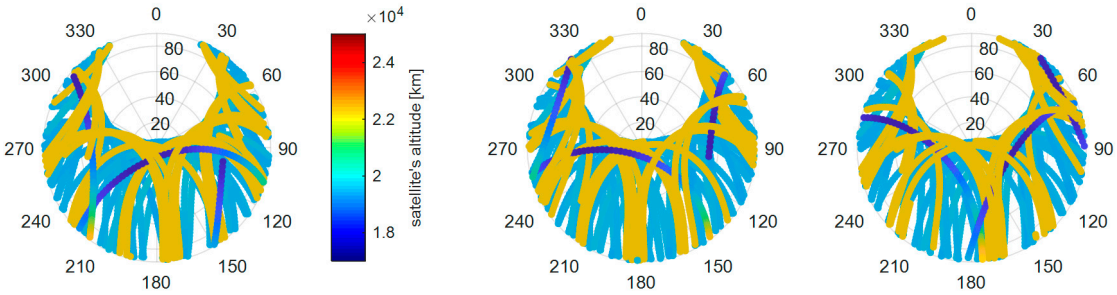

Figure 7. Sky plots of Galileo (dark yellow), Galileo E14 & E18 (dark blue) and GPS (azure) satellites with relation to its altitude over OLSZ station during the test period (3, 4, 5 October 2017, from left to right).

3.2.3. Performance Assessment of Instantaneous Positioning

We start the evaluation of the processing results with the ambiguity resolution domain. A GPS-based instantaneous solution results in a very high level of the ambiguity resolution success rate, from 97% to 99%. Therefore, no significant improvement triggered by the addition of the Galileo signals should be expected. The solution based on the Galileo-only constellation experienced a significantly lower success rate. ASR in this case did not exceed 33%, which may be attributed to the current Galileo constellation, and consequently, the number of tracked satellites resulting in high PDOP. A similar effect on short-baseline Galileo processing was found in other studies [27]. In that case, researchers indicated the important impact of the multipath effect and, therefore, applying multipath corrections resulted in a significant enhancement of the ambiguity fixing reliability.

According to our results, we did not, in turn, notice a significant influence on the ambiguity resolution success rate caused by the application or elimination of two Galileo satellites with incorrect orbits. On the first day of the experiment we obtained the same level of this percentage (96%) for both multi-constellation solutions (scenarios #3 and #4). On the next days, this discrepancy was at an insignificant level (1–2%). Comparing the ambiguity success rate from the coupled solution including Galileo satellites with incorrect orbits (#3) with that from the solution excluding them (#4), we can judge that the signals from these satellites did not noticeably influence the quality of the ambiguity resolution process.

In the following, the positioning results in coordinate domain are discussed. Table 5 summarises the standard deviations of fixed solution derived for consecutive scenarios, whereas Figure 8 shows the scatter plots of single-epoch coordinate residuals for a sample day (3 October 2017). The highest precision of coordinates was obtained with the use of a sole GPS constellation. In this case the standard deviation reached 0.9–1.2 cm, 0.6 cm, and 2.0–2.8 cm for the N, E and U components, respectively (Table 5). The results are in agreement with previous studies where researchers indicated the higher accuracy of a single-constellation GPS-based solution than for combined ones using Galileo or BDS [61–63]. Looking at the Galileo-based solution, we can clearly see the deterioration of the precision of height component, since the *std* reached 5.5–6.6 cm on 3–4 October 2017 and 12.8 cm on the last day of the experiment. On the other hand, plane coordinates were determined with only a slightly lower precision with respect to the GPS-based solution. In these cases, the *std* of N, E components was in the range of 1.5–1.7 cm and 1.2–1.4 cm, respectively. Since higher deterioration was observed in the height component, this may indicate that poor satellite geometry is the main source of this phenomenon.

Looking at the precision of the solutions based on coupled GPS + Galileo signals, again we cannot detect any significant impact on the coordinate domain caused by signals from a pair of Galileo FOC satellites with incorrect orbits. The discrepancies between *std* of fixed coordinates did not exceed 1 mm for horizontal components, whereas in the case of height this difference reached 6 mm on 3 October (Table 4). We, however, do not link this with the quality of E14 & E18 satellite signals, but with unfavourable Galileo satellites geometry.

Having investigated the results in the ambiguity resolution and coordinate domains, the following analysis was based on the observation residuals. Here we focus on the residuals corresponding to dual-frequency phase signals. Close attention was paid to the observations of the Galileo E14 and E18 satellites. At this point we should recall that the residuals correspond to double-differenced observables.

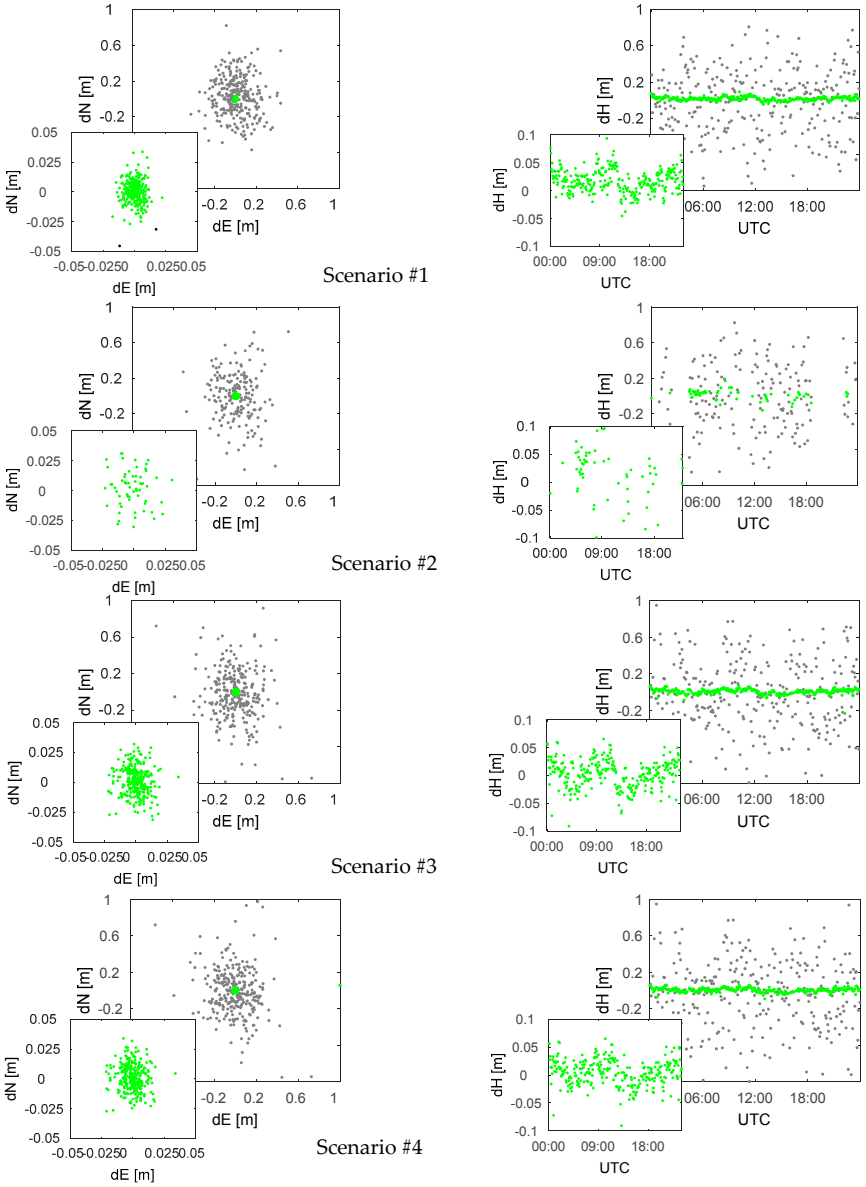

Figure 8. Scatter plots of coordinate residuals obtained on 3 October 2017 for tested scenarios. Grey and green dots represent float and fixed solutions, respectively.

Table 5. Empirical standard deviation (in cm) of the rover coordinates obtained in fixed solution.

	GPS	Galileo	GPS + Galileo with E14 & E18	GPS + Galileo without E14 & E18 Satellites
			3 October 2017 (276 DOY)	
N	0.9	1.5	1.2	1.1
E	0.6	1.2	0.8	0.8
U	2.1	5.5	2.9	2.3
			4 October 2017 (277 DOY)	
N	0.9	1.7	1.2	1.1
E	0.6	1.4	0.8	0.8
U	2.0	6.6	2.5	2.5
			5 October 2017 (278 DOY)	
N	1.2	1.9	1.3	1.3
E	0.6	1.3	0.9	0.9
U	2.8	12.8	3.3	3.4

As an example, Figures 9 and 10 show L1/E1 and L2/E5a phase residuals obtained on 3 October 2017. For better distinction, these values were depicted with separate colours for GPS, Galileo, E14 and E18 signals. Moreover, Figure 11 presents L1/E1 phase residuals in the function of satellite elevation and Figure 12 depicts elevation angle of the E14 and E18 satellites. In general, the figures did not reveal important differences in DD observable residuals between GPS, Galileo, E14 and E18 satellites. We did not recognise the outliers in the signals from the FOC satellites with incorrect orbits. A more detailed analysis may be performed on the basis of residuals' histograms and selected statistical measures. The former are presented in Figure 13. The latter were given in Table 6.

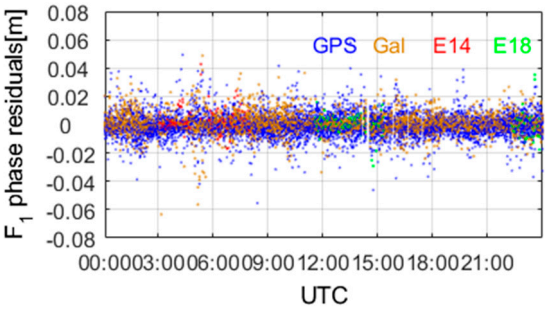

Figure 9. L1 + E1 DD phase residuals on 3 October 2017.

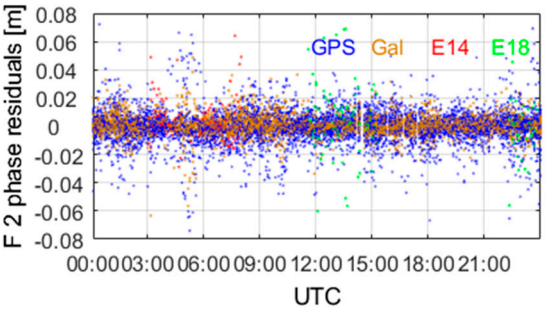

Figure 10. L2 + E5a DD phase residuals on 3 October 2017.

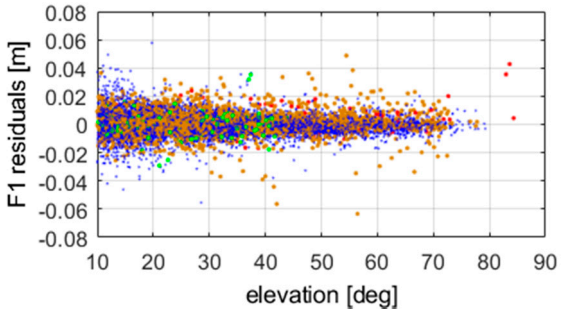

Figure 11. L1 + E1 DD phase residuals in the function of satellite elevation angle on 3 October 2017.

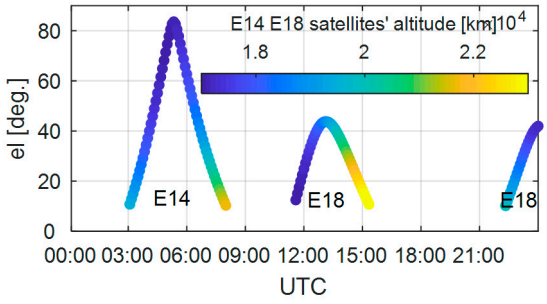

Figure 12. Elevation of the E14 and E18 satellites in the function of the satellite altitude on 3 October 2017.

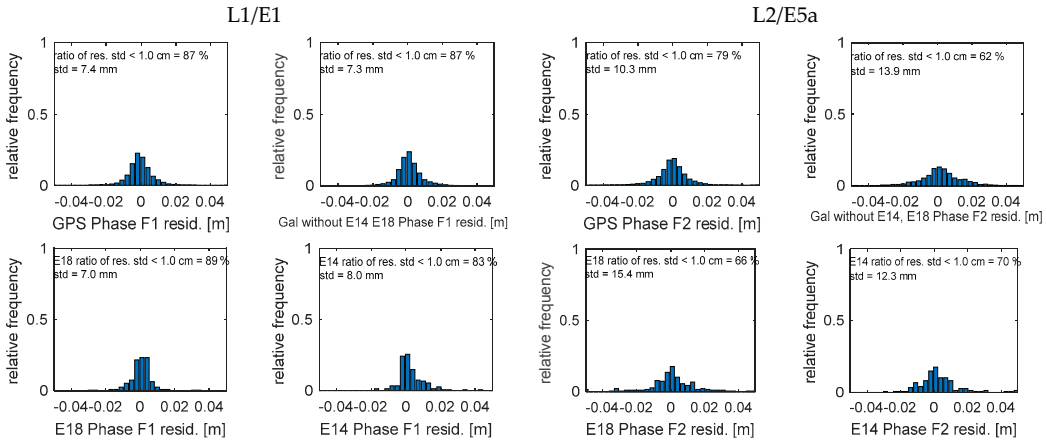

Figure 13. Histograms of phase residuals corresponding to L1/E1 and L2/E5a on 3 October 2017.

Table 6. Empirical standard deviation of phase observable residuals based on multi-baseline single-epoch solution (in mm).

	GPS L1	GPS L2	Gal E1	E14 E1	E18 E1	Gal E5a	E14 E5a	E18 E5a
3 October	7.4	10.3	7.3	8.0	7.0	13.9	12.3	15.4
4 October	7.0	10.3	7.3	8.7	7.5	14.6	16.3	15.8
5 October	7.8	10.3	7.7	8.5	6.5	14.6	17.3	14.7

Table 6 summarises the results in the observation residuals domain obtained with scenario #3. Specifically, we give the values of the standard deviation of phase residuals obtained on the corresponding days of the positioning experiment. In addition, Figure 13 visualises the distribution of the phase residuals of the selected satellites and systems obtained on 3 October 2017.

As we can see from Table 6, the standard deviation of the L1/E1 phase residuals, corresponding to GPS, Galileo, E14 and E18 signals, were at a comparable level, in the range of 6.5–8.7 mm. Slightly

higher values were recognised for residuals of double-differenced observables formed with the application of E14 satellites (up to 8.7 mm), whereas in the case of E18 signals these indicators were in the range of 6.5–7.5 mm. At the same time the *std* for observables formed with Galileo satellites other than E14 & E18 were within 7.3–7.7 mm. According to this, we do not see important differences between residuals corresponding to signals of satellites with incorrect orbit and others. In the case of L2 and E5a frequencies, we found that the *std* of phase residuals was at a higher level with respect to L1/E1. This may be explained in two ways. First, the weighting scheme distinguishes the observable weights between frequencies. Specifically, the weights are correlated to the ratio of applied frequencies with respect to L1/E1 [64]. Therefore, L2 and E5a signals are depicted with lower weights than L1/E1. This ratio is obviously more significant when E1 & E5a signals are used than in the case of L1 & L2. Moreover, we should note the lack of official antenna phase centre offsets and variations for E5a signals. In this case, corrections corresponding to L2 frequency are applied. For GPS signals the *std* of L2 phase residuals equalled 10.3 mm, whereas this reached 14.6 mm in the case of Galileo satellite signals excluding E14 and E18. In the case of the latter satellites, the standard deviation of the E5a phase residuals of DD observables was in the range 12.3–17.3 mm. Judging on the basis of observable residuals, the FOC satellites with incorrect orbits did not stand out.

4. Summary and Conclusions

This contribution evaluates the performance of the coupled Galileo + GPS instantaneous medium-range positioning, with special attention paid to the application of the Galileo FOC satellites—E14 & E18—launched into incorrect elliptic orbital planes. Therefore, the main goal of the paper was to investigate the potential capability of these satellites in surveying and geodetic applications. In the paper we provided both a methodology of coupled instantaneous medium-range positioning and experimental performance analysis.

In the first part of the study, we focused on the analysis of the signal power and noise of Galileo E14 & E18 satellites, comparing the results to other GPS and Galileo satellites. It was confirmed that the signal power of E14 & E18 satellites was basically higher than the signals of other Galileo satellites (up to 53 dB-Hz). This was clearly related to their lower orbital altitude over the area of the test stations. On the other hand, analysis of observational noise did not reveal any differences between all the European satellites. The inter-system comparison of the noise (GPS and Galileo) proved that the precision of code measurement of the latter was significantly better. The same effect, though less pronounced, was also observed in triple-frequency combination of phase observations.

Further analysis was based on the positioning experiment and considered ambiguity resolution and coordinate domains as well as observable residuals. We confirmed the high performance of the instantaneous medium-range positioning based on the GPS-only constellation, providing unobstructed visibility of the satellites. When adding in Galileo observations, we did not see an important change in the performance of the ambiguity resolution. Both solutions, GPS and GPS + Galileo, provided competitive rates of ambiguity resolution success, reaching up to 99%. On the basis of the two scenarios, one with and one without E14 & E18 satellites, we found that the Galileo satellites launched into eccentric orbital planes did not deteriorate the ambiguity resolution process. On the other hand, we experienced significant worsening in the ambiguity domain when the Galileo-only constellation was applied. We believe that this was caused by the current uncompleted constellation and thus poor geometry of the Galileo satellites over the experimental area.

Having analysed the precision of the solutions based on the coupled GPS + Galileo constellation, we can conclude that the E14 & E18 satellites do not have any negative impact on the coordinate domain. The differences between the standard deviation of fixed coordinates did not exceed 1 mm for plane components, whereas in the case of height this difference reached 6 mm.

According to the obtained results, again we do not see any increased observation residuals corresponding to signals of E14 and E18. The standard deviation of the L1/E1 phase residuals

corresponding to GPS, Galileo and E14 & E18 satellite signals were at a comparable level, in the range of 6.5–8.7 mm.

Considering the above, precise positioning using Galileo satellites launched into incorrect orbital planes is feasible. Therefore, these satellites are applicable to most geodetic, surveying and many other solutions. This claim, however, holds true providing the precise ephemeris of the satellites.

Acknowledgments: The work in this contribution was supported by the National Science Centre, Poland: project No. 2016/23/D/ST10/01546. The GNSS observational data from CORS network were kindly provided by VRSNet Ltd., Poland.

Author Contributions: Jacek Paziewski designed and performed the experiments, analysed the data and discussed the conclusions. Rafal Sieradzki performed and analysed the experiment given in Section 2 and discussed the conclusions. Pawel Wielgosz supervised the investigations and discussed the conclusions.

Conflicts of Interest: The authors declare no conflict of interest.

References

1. Falcone, M.; Lugert, M.; Malik, M.; Crisci, M.; Rooney, E.; Jackson, C.; Threteway, M. GIOVE-A In Orbit Testing Results. In Proceedings of the 19th International Technical Meeting of the Satellite Division of The Institute of Navigation (ION GNSS 2006), Fort Worth, TX, USA, 26–29 September 2006; pp. 1535–1546.
2. European Union. *European GNSS (Galileo) Open Service Signal in Space Interface Control Document*; Issue 1.2; OS SIS ICD; European Union: Brussels, Belgium, 2015.
3. European Union. *European GNSS (Galileo) Galileo Open Service Service Definition Document*; Issue 1.0, OS SSD; European Union: Brussels, Belgium, 2016.
4. Steigenberger, P.; Hauschild, A. First Galileo FOC Satellite on the Air—Will Be Employable for Surveying, Precise Positioning, and Geodesy. *GPS World* **2015**, *26*, 8–12.
5. Sosnica, K.; Prange, L.; Kazmierski, K.; Bury, G.; Drozdzewski, M.; Zajdel, R.; Hadas, T. Validation of Galileo orbits using SLR with a focus on satellites launched into incorrect orbital planes. *J. Geodesy* **2017**, *12*, 1–18. [CrossRef]
6. Ashby, N. Relativity in the global positioning system. *Living Rev. Relat.* **2003**, *6*, 1. [CrossRef] [PubMed]
7. Delva, P.; Hees, A.; Bertone, S.; Richard, E.; Wolf, P. Test of the gravitational redshift with stable clocks in eccentric orbits: Application to Galileo satellites 5 and 6. *Class. Quantum Gravity* **2015**, *32*, 232003. [CrossRef]
8. Delva, P.; Puchades, N. Testing the gravitational redshift with eccentric Galileo satellites. *Proceedings of the 6th International Colloquium Scientific and Fundamental Aspects of the GNSS/Galileo, Valencia, Spain, 25–27 October 2017*; Technical University of Valencia: Valencia, Spain, 2017.
9. Simsky, A.; Mertens, D.; Sleewaegen, J.M.; Hollreiser, M.; Crisci, M. Experimental results for the multipath performance of galileo signals transmitted by GIOVE—A satellite. *Int. J. Navig. Obs.* **2008**, *2008*, 13. [CrossRef]
10. De Bakker, P.F.; van der Marel, H.; Tiberius, C.C.J.M. Geometry free undifferenced, single and double differenced analysis of single-frequency GPS, EGNOS, and GIOVE-A/B measurements. *GPS Solut.* **2009**, *13*, 305–314. [CrossRef]
11. De Bakker, P.F.; Tiberius, C.C.J.M.; van der Marel, H.; van Bree, R.J.P. Short and zero baseline analysis of GPS L1 C/A, L5Q, GIOVE E1B, and E5aQ signals. *GPS Solut.* **2012**, *16*, 53–64. [CrossRef]
12. Cai, C.; He, C.; Santerre, R.; Pan, L.; Cui, X.; Zhu, J. A comparative analysis of measurement noise and multipath for four constellations: GPS, BeiDou, GLONASS and Galileo. *Surv. Rev.* **2016**, *48*, 287–295. [CrossRef]
13. Odijk, D.; Teunissen, P.J.G.; Khodabandeh, A. Galileo IOV RTK positioning: Standalone and combined with GPS. *Surv. Rev.* **2014**, *46*, 267–277. [CrossRef]
14. Steigenberger, P.; Hugentobler, U.; Montenbruck, O. First demonstration of Galileo-only positioning. *GPS World* **2013**, *24*, 14–15.
15. Cai, C.; Luo, X.; Liu, Z.; Xiao, Q. Galileo signal and positioning performance analysis based on four IOV satellites. *Navigation* **2014**, *67*, 810–824. [CrossRef]
16. Gioia, C.; Borio, D.; Angrisano, A.; Gaglione, S.; Fortuny-Guasch, J. A Galileo IOV assessment: Measurement and position domain. *GPS Solut.* **2015**, *19*, 187–199. [CrossRef]
17. Steigenberger, P.; Montenbruck, O. Galileo status: Orbits, clocks, and positioning. *GPS Solut.* **2017**, *21*, 319–331. [CrossRef]

18. Pan, L.; Cai, C.; Santerre, R.; Zhang, X. Performance evaluation of single-frequency point positioning with GPS, GLONASS, BeiDou and Galileo. *Surv. Rev.* **2017**, *70*, 465–482. [CrossRef]
19. Tegedor, J.; Øvstedal, O.; Vigen, E. Precise orbit determination and point positioning using GPS, Glonass, Galileo and BeiDou. *J. Geod. Sci.* **2014**, *4*, 65–73. [CrossRef]
20. Afifi, A.; El-Rabbany, A. Single frequency GPS/Galileo precise point positioning using Un-differenced and between-satellite single difference measurements. *Geomatica* **2014**, *68*, 195–205. [CrossRef]
21. Afifi, A.; El-Rabbany, A. An innovative dual frequency PPP model for combined GPS/Galileo observations. *J. Appl. Geodesy* **2015**, *9*, 27–34. [CrossRef]
22. Cai, C.; Gao, Y.; Pan, L.; Zhu, J. Precise point positioning with quad-constellations: GPS, BeiDou, GLONASS and Galileo. *Adv. Space Res.* **2015**, *56*, 133–143. [CrossRef]
23. Li, X.; Li, X.; Yuan, Y.; Zhang, K.; Zhang, X.; Wickert, J. Multi-GNSS phase delay estimation and PPP ambiguity resolution: GPS, BDS, GLONASS, Galileo. *J. Geodesy* **2017**, 1–30. [CrossRef]
24. Odijk, D.; Teunissen, P.J.G.; Huisman, L. First results of mixed GPS&GIOVE single-frequency RTK in Australia. *J. Spat. Sci.* **2012**, *57*, 3–18.
25. Odolinski, R.; Teunissen, P.J.G.; Odijk, D. Combined BDS, Galileo, QZSS and GPS single-frequency RTK. *GPS Solut.* **2015**, *19*, 151–163. [CrossRef]
26. Paziewski, J.; Wielgosz, P. Investigation of some selected strategies for multi-GNSS instantaneous RTK positioning. *Adv. Space Res.* **2017**, *59*, 12–23. [CrossRef]
27. Zaminpardaz, S.; Teunissen, P.J.G. Analysis of Galileo IOV + FOC signals and E5 RTK performance. *GPS Solut.* **2017**, *21*, 1855–1870. [CrossRef]
28. Hernandez-Pajares, M.; Juan, J.; Sanz, J.; Colombo, L. Feasibility of wide-area sub-decimeter navigation with GALILEO and modernized GPS. *IEEE Trans. Geosci. Remote Sens.* **2003**, *41*, 2128–2131. [CrossRef]
29. Wielgosz, P.; Kashani, I.; Grejner-Brzezinska, D.A. Analysis of long-range network RTK during a severe ionospheric storm. *J. Geodesy* **2005**, *79*, 524–531. [CrossRef]
30. Hernandez-Pajares, M.; Juan, J.M.; Sanz, J.; Aragon-Angel, A.; Ramos-Bosch, P.; Odijk, D.; Teunissen, P.J.G.; Samson, J.; Tossaint, M.; Albertazzi, M. Wide-Area RTK: High Precision Positioning on a Continental Scale. *Inside GNSS* **2010**, *5*, 35–46.
31. Juan, J.M.; Sanz, J.; Hernández-Pajares, M.; Samson, J.; Tossaint, M.; Aragón-Àngel, A.; Salazar, D. Wide Area RTK: A satellite navigation system based on precise real-time ionospheric modelling Radio Science. *Radio Sci.* **2012**, *47*. [CrossRef]
32. Paziewski, J.; Wielgosz, P. Assessment of GPS + Galileo and multi-frequency Galileo single-epoch precise positioning with network corrections. *GPS Solut.* **2014**, *18*, 571–579. [CrossRef]
33. El-Mowafy, A.; Deo, M.; Rizos, C. On biases in Precise Point Positioning with multi-constellation and multi-frequency GNSS data. *Meas. Sci. Technol.* **2016**, *27*, 035102. [CrossRef]
34. Choy, S.; Bisnath, S.; Rizos, C. Uncovering common misconceptions in GNSS Precise Point Positioning and its future prospect. *GPS Solut.* **2017**, *21*, 13–22. [CrossRef]
35. Odijk, D.; Nadarajah, N.; Zaminpardaz, S. GPS, Galileo, QZSS and IRNSS differential ISBs: Estimation and application. *GPS Solut.* **2017**, *21*, 439–450. [CrossRef]
36. Paziewski, J.; Wielgosz, P. Accounting for Galileo-GPS inter-system biases in precise satellite positioning. *J. Geodesy* **2015**, *89*, 81–93. [CrossRef]
37. Paziewski, J.; Sieradzki, R.; Wielgosz, P. Selected properties of GPS and Galileo-IOV receiver Inter System Biases in multi GNSS data processing. *Meas. Sci. Technol.* **2015**, *26*, 095008. [CrossRef]
38. Bock, Y.; Nikolaidis, R.; de Jonge, P.J.; Bevis, M. Instantaneous geodetic positioning at medium distances with the Global Positioning System. *J. Geophys. Res.* **2000**, *105*, 28233–28253. [CrossRef]
39. Odijk, D. Instantaneous precise GPS positioning under geomagnetic storm conditions. *GPS Solut.* **2001**, *5*, 29–42. [CrossRef]
40. Kashani, I.; Grejner-Brzezinska, D.A.; Wielgosz, P. Towards Instantaneous Network-Based RTK GPS Over 100 km Distance. *Navigation* **2005**, *52*, 239–245. [CrossRef]
41. Genrich, J.F.; Bock, Y. Instantaneous geodetic positioning with 10–50 Hz GPS measurements: Noise characteristics and implications for monitoring networks. *J. Geophys. Res.* **2006**, *111*, B03403. [CrossRef]
42. Próchniewicz, D.; Szpunar, R.; Brzeziński, A. Network-Based Stochastic Model for instantaneous GNSS real-time kinematic positioning. *J. Surv. Eng.* **2016**, *142*, 05016004. [CrossRef]

43. Brunner, F.K.; Hartinger, H.; Troyer, L. GPS signal diffraction modelling: The stochastic SIGMAΔ model. *J. Geodesy* **1999**, *73*, 259–267. [CrossRef]
44. Wieser, A.; Brunner, F.K. An Extended Weight Model for GPS Phase Observations. *Earth Planets Space* **2000**, *52*, 777–782. [CrossRef]
45. Montenbruck, O.; Hauschild, A.; Steigenberger, P.; Hugentobler, U.; Teunissen, P.; Nakamura, S. Initial assessment of the COMPASS/BeiDou-2 regional navigation satellite system. *GPS Solut.* **2013**, *17*, 211–222. [CrossRef]
46. Hauschild, A.; Montenbruck, O.; Sleewaegen, J.M.; Huisman, L.; Teunissen, P.J.G. Characterization of Compass M-1 signals. *GPS Solut.* **2012**, *16*, 117–126. [CrossRef]
47. Estey, L.H.; Meertens, C.M. TEQC: The multi-purpose toolkit for GPS/GLONASS data. *GPS Solut.* **1999**, *3*, 42–49. [CrossRef]
48. Montenbruck, O.; Hugentobler, U.; Dach, R.; Steigenberger, P.; Hauschild, A. Apparent clock variations of the Block IIF-1 (SVN62) GPS satellite. *GPS Solut.* **2011**, *16*, 303–313. [CrossRef]
49. Julien, O.; Cannon, M.E.; Alves, P.; Lachapelle, G. Triple frequency ambiguity resolution using GPS/Galileo. *Eur. J. Navig.* **2004**, *2*, 51–56.
50. Gao, W.; Gao, C.; Pan, S.; Meng, X.; Xia, Y. Inter-System Differencing between GPS and BDS for Medium-Baseline RTK Positioning. *Remote Sens.* **2017**, *9*, 948. [CrossRef]
51. Bock, Y.; Gourevitch, S.A.; Counselman, C.C.; King, R.W.; Abbot, R.I. Interferometric analysis of GPS phase observations. *Manuscr. Geodaet.* **1986**, *11*, 282–288.
52. Teunissen, P.J.G. The geometry-free GPS ambiguity search space with a weighted ionosphere. *J. Geodesy* **1997**, *71*, 370–383. [CrossRef]
53. Wielgosz, P. Quality assessment of GPS rapid static positioning with weighted ionospheric parameters in generalized least squares. *GPS Solut.* **2011**, *15*, 89–99. [CrossRef]
54. Paziewski, J. Study on desirable ionospheric corrections accuracy for network-RTK positioning and its impact on time-to-fix and probability of successful single-epoch ambiguity resolution. *Adv. Space Res.* **2016**, *57*, 1098–1111. [CrossRef]
55. Paziewski, J. Precise GNSS single epoch positioning with multiple receiver configuration for medium-length baselines: Methodology and performance analysis. *Meas. Sci. Technol.* **2015**, *26*, 035002. [CrossRef]
56. Odijk, D. Weighting Ionospheric Corrections to Improve Fast GPS Positioning Over Medium Distances. In Proceedings of the 13th International Technical Meeting of the Satellite Division of the Institute of Navigation (ION GPS 2000), Salt Lake City, UT, USA, 19–22 September 2000.
57. Prange, L.; Orliac, E.; Dach, R.; Arnold, D.; Beutler, G.; Schaer, S.; Jäggi, A. CODE's five-system orbit and clock solution—The challenges of multi-GNSS data analysis. *J. Geodesy* **2017**, *91*, 345–360. [CrossRef]
58. Chang, X.W.; Yang, X.; Zhou, T. MLAMBDA: A modified LAMBDA method for integer least-squares estimation. *J. Geodesy* **2005**, *79*, 552–565. [CrossRef]
59. Wang, J.; Stewart, M.; Tsakiri, M. A discrimination test procedure for ambiguity resolution on-the-fly. *J. Geodesy* **1998**, *72*, 644–653. [CrossRef]
60. Available online: http://vrsnet.pl (accessed on 20 October 2017).
61. He, H.; Li, J.; Yang, Y.; Xu, J.; Guo, H.; Wang, A. Performance assessment of single- and dual-frequency Beidou/GPS single-epoch kinematic positioning. *GPS Solut.* **2014**, *18*, 393–403. [CrossRef]
62. Deng, C.; Tang, W.; Liu, J.; Shi, C. Reliable single-epoch ambiguity resolution for short baselines using combined GPS/Beidou system. *GPS Solut.* **2014**, *18*, 375–386. [CrossRef]
63. Paziewski, J.; Sieradzki, R. Integrated GPS+BDS instantaneous medium baseline RTK positioning: Signal analysis, methodology and performance assessment. *Adv. Space Res.* **2017**, *60*, 2561–2573. [CrossRef]
64. Han, S. Quality-control issues relating to instantaneous ambiguity resolution for real-time GPS kinematic positioning. *J. Geodesy* **1997**, *71*, 351–361. [CrossRef]

© 2018 by the authors. Licensee MDPI, Basel, Switzerland. This article is an open access article distributed under the terms and conditions of the Creative Commons Attribution (CC BY) license (http://creativecommons.org/licenses/by/4.0/).